FINITE ELEMENT MODEL VERIFICATION FOR THE USE OF PIEZOELECTRIC SENSOR IN STRUCTURAL MODAL ANALYSIS

B.-T. Wang [*] **P.-H. Chen**[**]

Department of Mechanical Engineering
National Pingtung University of Science and Technology
Pingtung, Taiwan 91201, R.O.C.

R.-L. Chen [***]

Center for Measurement Standards
Industrial Technology Research Institute
Hsinchu, Taiwan 31040, R.O.C.

ABSTRACT

This paper presents the theoretical modal analysis for the use of PVDF sensor in structural modal testing via finite element analysis (FEA). A series of rectangular PVDF films are adhered on the surface of cantilever beam as sensors, while the point impact force is applied as the actuator for experimental modal analysis (EMA). Natural frequencies and mode shapes determined from both FEA and EMA are validated. In FEA, the beam structure is modeled by 3D solid elements, and the PVDF films are modeled by 3D coupled field piezoelectric elements. Both modal analysis and harmonic response analysis are performed to obtain the structural modal parameters and frequency response functions, respectively. Results show that both FEA and EMA results agree well. In particular, the PVDF sensor mode shapes, proportional to the slope difference between the two edges of PVDF film, are numerically and experimentally validated by FEA and EMA, respectively. Therefore, the simulation of PVDF films for vibration analysis in FEA can be verified and easily extended to other complex structures that may contain piezoelectric materials.

Keywords : Finite element model, PVDF film, Experimental modal analysis, Vibration analysis.

1. INTRODUCTION

The piezoelectric materials have been drawn many interests for the use as sensors and actuators. Hubbard [1] introduced the rectangular shape of PVDF (Polyvinylidene Fluoride) film for the application to vibration control of beam structures as the sensor. Lee and Moon [2] and Collin *et al*. [3] developed special shape of PVDF films to sense the specific vibration modal response as known modal sensors. Galea *et al*. [4] applied the PVDF film as the sensor to the structural fault diagnosis and health monitoring. Collet and Jezequel [5] and Tanaka *et al*. [6] utilized the similar configuration of PVDF film as modal filters for vibration control.

There have been many researches using finite element method to analyze piezoelectric structures. Allik and Hughes [7] applied the finite element method to analyze the three-dimensional piezoelectric vibration modes. The finite element formulation included the piezoelectric and electroelastic effect. A tetrahedral finite element was also presented based on three-dimensional electroelasticity. Boucher *et al*. [8] developed a perturbation method to numerically determine the eigenmodes of vibration for piezoelectric transducers. The three-dimensional finite element method was formulated to predict the piezoelectric transducer resonance and antiresonance frequencies as well as sound radiation for different sizes of the PZT cubes. Kunkel *et al*. [9] applied the finite element method to calculate the natural vibration modes of the piezoelectric ceramic disks. To optimize the disk geometry, the dependence of the vibration mode on the disk diameter-to-thickness ratio was studied. Ha *et al*. [10] modeled laminated composite structures containing distributed piezoelectric ceramic sensors and actuators by finite element analysis. The computer code was developed to analyze the mechanical-electrical response of the piezoelectric ceramic laminated composites. Experiments were also conducted to verify the computer simulations. The comparisons between predicted and experimental results

* Professor ** Graduate student *** Associate Engineer

agreed well. There were also many researches via finite element analysis about piezoelectric ultrasonic transducers and piezoelectric transformers such as Kagawa and Yamabuchi [11], Challande [12] and Tsuchiya and Kagawa [13].

The adoption of piezoelectric transducers for structural modal testing is also drawn attention. Sun *et al*. [14] derived the frequency response function (FRF) through electric admittance of piezoelectric transducers for obtaining the dynamic parameters of beam structures. However, they did not physically interpret those dynamic parameters. Norwood [15] successfully applied both the impact hammer and PVDF film as actuation sources, respectively, to modal testing of cylindrical shell structures. Wang [16] derived the frequency response functions between the traditional and piezoelectric transducers for simply supported beam. He introduced the feasibility of the use of piezoelectric transducers for structural modal testing.

Wang [17] generalized the formulation of frequency response functions (FRFs) for continuous structure systems subject to various forms of actuators and sensors. The actuator and sensor eigenfunctions (mode shapes) were respectively identified and physically interpreted according to the testing procedures, either roving the actuator or the sensor. Wang's work provided with the theoretical base for the application of smart materials, such as PZT actuators and PVDF sensors, to smart structural testing. Wang and Wang [18] theoretically demonstrated the feasibility of using piezoelectric transducers for cantilever beam modal testing. An array of finite-length PVDF films was assumed to be equally spaced and distributed over the beam acting as sensors, while a fixed pure-bending PZT actuator was served as actuation force. They performed synthetic modal analysis to extract modal parameters of the beam by using piezoelectric transducers. Wang [19] also applied the similar arrangement of an array of PVDF sensors on a cantilever beam and developed a novel wave number domain sensing technique for active structural acoustic control (ASAC). Nevertheless, there have had no experimental validation yet. Therefore, one of the objectives for this work is to experimentally verify such a sensor arrangement for structural testing and can lead to ASAC as well.

This paper validates the use of PVDF film sensors for structural modal testing of cantilever beam by both finite element method and experimental approach. First, a brief introductory of theoretical modal analysis for cantilever beam with distributed PVDF film sensors is summarized. Second, the finite element modeling of the cantilever beam containing PVDF film is presented and solved by finite element code, ANSYS. The experimental modal analysis by using impact hammer as the actuator and the distributed PVDF film as the sensor is then performed with the testing procedure, fixed the actuator and roving the sensor. Finally, the theoretical and FEA simulation results are compared with those from experiments. FRFs and modal parameters are presented to validate the finite element model. This work thus leads to the simulation of PVDF sensors interacted with structures in FEA and can be easily extended to other complex structures such as plates or shells.

2. THEORETICAL ANALYSIS

This work adopts evenly distributed PVDF film sensors adhered onto cantilever beam as shown in Fig. 1 for structural modal testing, while the point force is applied as the actuation source. The arrangement and coordinates of the *i*-th PVDF sensor and the *j*-th point force on the beam is depicted in Fig. 2. A brief review of theoretical analysis for cantilever beam with distributed piezoelectric transducers is summarized [18]. From free vibration analysis, the natural frequencies and the corresponding displacement mode shape functions of a cantilever beam can be identified as follows [20]:

$$\omega_n = 2\pi f_n = (\alpha_n L_b)^2 \sqrt{\frac{E_b I_b}{\rho_b b_b t_b L_b^4}} = \alpha_n^2 \sqrt{\frac{E_b I_b}{\rho_b b_b t_b}} \tag{1}$$

$$\phi_n(x) = \cosh \alpha_n x - \cos \alpha_n x - \sigma_n(\sinh \alpha_n x - \sin \alpha_n x) \tag{2}$$

where

$$\sigma_n = \frac{\sinh \alpha_n L_b - \sin \alpha_n L_b}{\cosh \alpha_n L_b + \cos \alpha_n L_b} \tag{3}$$

The eigenvalue (α_n, n = 1, 2, …) can be obtained as follows [21]

$$\begin{aligned} \alpha_1 L_b &= 1.875104 \\ \alpha_2 L_b &= 4.694091 \\ \alpha_3 L_b &= 7.854757 \\ \alpha_4 L_b &= 10.995540 \\ \alpha_5 L_b &= 14.137168 \\ &\vdots \end{aligned} \tag{4}$$

for $n > 5$, $\alpha_n L_b \approx \dfrac{(2n-1)\pi}{2}$

A strip of PVDF film can be applied as the sensing device as shown in Fig. 2. The FRF between the measured voltage of the *i*-th PVDF sensor, V_i, and the force amplitude applied by the *j*-th point force, F_j, can be obtained as follows [17]:

$$\alpha_{v_i f_j}(\omega) = \frac{V_i}{F_j} = \sum_{n=1}^{\infty} \frac{\phi_{n,i}^{v} \, \phi_{n,j}^{f}}{(\omega_n^2 - \omega^2) + i(2\xi_n \omega_n \omega)} \tag{5}$$

where

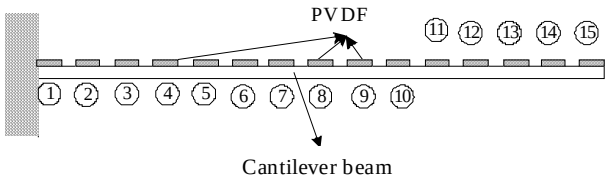

Fig. 1 The arrangement of the PVDF sensors on the cantilever beam

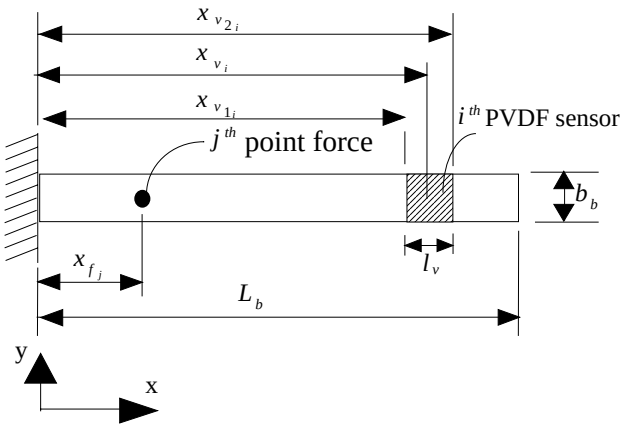

Fig. 2 The arrangement of coordinate on the cantilever beam

$$\phi_{n,j}^{f} = \frac{1}{\sqrt{\rho_b\, b_b\, t_b\, L_b}}\phi_n(x_{f_j}) \tag{6}$$

$$\phi_{n,i}^{v} = \frac{1}{\sqrt{\rho_b\, b_b\, t_b\, L_b}} k_v[\phi_n'(x_{v2_i}) - \phi_n'(x_{v1_i})] \tag{7}$$

$$k_v = \frac{t_v}{\varepsilon A_v}\frac{t_b + t_v}{2} l_v\, e_{31} \tag{8}$$

$\phi_{n,i}^{v}$ and $\phi_{n,j}^{f}$ represents the values of the *n*-th PVDF sensor and hammer actuator mode shape functions at the *i*-th and *j*-th location of the PVDF sensor and hammer actuator, respectively. Wang [17] have shown that the testing procedure in EMA will determine the extracted mode shapes being actuator or sensor mode shapes. In this work, the hammer actuator is fixed, and the PVDF sensors are roving in EMA. Therefore, the PVDF sensor mode shapes will be obtained. The PVDF mode shape functions are proportional to the slope difference between the two edges of PVDF film as shown in Eq. (7) and can be shown to be the mirror image of displacement mode shapes against the clamped end [18].

3. FINITE ELEMENT ANALYSIS

This section details the finite element modeling for the cantilever beam with distributed PVDF film sensors as shown in Fig. 1. There are 15 PVDF films adhered on the beam. Tables 1 and 2 show the physical properties of beam and PVDF film, respectively. The finite element model consisting of steel beam and PVDF films is built in ANSYS software and solved. Both modal analysis and harmonic response analysis are performed to determine the structural modal parameters and FRFs, respectively.

The piezoelectric material has the mechanical-electrical characteristic, and there are mechanical and dielectric items in the piezoelectric equation. The mechanical part has mechanical stress (*T*) and mechanical strain (*S*) parameters. The dielectric part has electrical field (*E*) and electric displacement (*D*) parameters. So, the piezoelectric equation has many types based on these parameters. The e type of the piezoelectric equation is shown as follows [22]:

$$T_p = c_{pq}^{E} S_q - e_{kp} E_k \tag{9}$$

$$D_i = e_{iq} S_q + \varepsilon_{ik}^{S} E_k \tag{10}$$

where $p = q = 6$, $i = k = 3$.

The elastic constants of piezoelectric material can be expressed as follows:

$$[c] = \begin{bmatrix} c_{11} & c_{12} & c_{13} & 0 & 0 & 0 \\ & c_{22} & c_{23} & 0 & 0 & 0 \\ & & c_{33} & 0 & 0 & 0 \\ & & & c_{44} & 0 & 0 \\ & \text{Symmetric} & & & c_{55} & 0 \\ & & & & & c_{66} \end{bmatrix} \tag{11}$$

Table 1 Physical properties of cantilever beam

Material	Steel
Length (L_b)	0.3m
Width (b_b)	0.04m
Thickness (t_b)	0.002m
Density (ρ_b)	8436kg/m^3
Young's Modulus (E_b)	180.2×10^9N/m^2
Poisson ratio (υ_b)	0.322

Table 2 Physical properties of PVDF sensor

Material	PVDF
Length (L_p)	0.01m
Width (b_p)	0.04m
Thickness (t_p)	54×10^{-6}m
Density (ρ_b)	1800kg/m^3
Young's Modulus (E_b)	2×10^9N/m^2
Poisson ratio (υ_b)	0.33
Piezoelectric field intensity constant (e_{31}, e_{32})	54×10^{-3}N/Vm
Permittivity (ε)	132.81×10^{-12}F/m

where $c_{66} = 2(c_{11} - c_{12})$, $c_{11} = c_{22}$, $c_{44} = c_{55}$, $c_{13} = c_{23}$.

The piezoelectric stress constants can be expressed as follows:

$$[e] = \begin{bmatrix} 0 & 0 & e_{31} \\ 0 & 0 & e_{32} \\ 0 & 0 & e_{33} \\ 0 & e_{24} & 0 \\ e_{15} & 0 & 0 \\ 0 & 0 & 0 \end{bmatrix} \tag{12}$$

where $e_{31} = e_{32}$, $e_{24} = e_{15}$.

The permittivity constants can be expressed as follows:

$$[\varepsilon] = \begin{bmatrix} \varepsilon_{11} & 0 & 0 \\ 0 & \varepsilon_{22} & 0 \\ 0 & 0 & \varepsilon_{33} \end{bmatrix} \tag{13}$$

where $\varepsilon_{11} = \varepsilon_{22}$.

The piezoelectric equation can then be expressed in matrix form as follows.

$$\begin{bmatrix} T_1 \\ T_2 \\ T_3 \\ T_4 \\ T_5 \\ T_6 \\ D_1 \\ D_2 \\ D_3 \end{bmatrix} = \begin{bmatrix} c_{11} & c_{12} & c_{13} & 0 & 0 & 0 & 0 & 0 & -e_{31} \\ c_{12} & c_{11} & c_{13} & 0 & 0 & 0 & 0 & 0 & -e_{31} \\ c_{13} & c_{13} & c_{33} & 0 & 0 & 0 & 0 & 0 & -e_{33} \\ 0 & 0 & 0 & \frac{(c_{11}-c_{12})}{2} & 0 & 0 & 0 & -e_{15} & 0 \\ 0 & 0 & 0 & 0 & c_{44} & 0 & -e_{15} & 0 & 0 \\ 0 & 0 & 0 & 0 & 0 & c_{44} & 0 & 0 & 0 \\ 0 & 0 & 0 & 0 & e_{15} & 0 & \varepsilon_{11} & 0 & 0 \\ 0 & 0 & 0 & e_{15} & 0 & 0 & 0 & \varepsilon_{11} & 0 \\ e_{31} & e_{31} & e_{33} & 0 & 0 & 0 & 0 & 0 & \varepsilon_{33} \end{bmatrix} \begin{bmatrix} S_1 \\ S_2 \\ S_3 \\ S_4 \\ S_5 \\ S_6 \\ E_1 \\ E_2 \\ E_3 \end{bmatrix} \tag{14}$$

The developed finite element model is depicted and shown in Fig. 3. There are two types of elements used in the model as listed in Table 3. The SOLID 45 element, a 3-D structural solid element, is used to construct the cantilever beam. There are 8 nodes in each element and 3 degree-of-freedom (DOF) on each node. The PVDF film is modeled by SOLID 5 element that can be used to model a 3D magnetic, thermal, electric, piezoelectric and structural field with coupling effects. In this work, the structural and piezoelectric analyses are employed, and thus the PVDF element has eight nodes with four DOFs, including three displacements (UX, UY, UZ) and electric voltage (VOLT), as listed in Table 3. For the consideration of element compatibility, the beam is modeled by SOLID 45 element that has the same structural DOFs. Therefore, there are no rotational displacements involved. Both SOLID 45 and SOLID 5 elements are used to model the cantilever beam and PVDF sensors, respectively. There are coupling effects on the interface between beam and PVDF sensors.

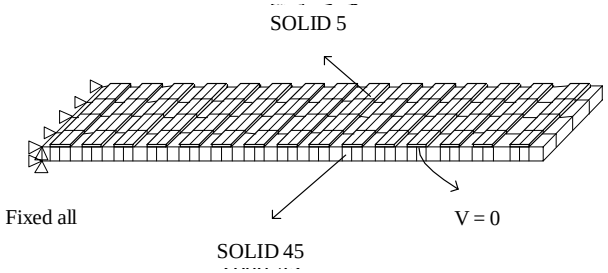

Fig. 3 The finite element model of the cantilever beam

Table 3 Properties of element type

Element type	Model	No. of node	Degree of Freedom
Solid 45	3-D Structural Solid	8	UX, UY, UZ
Solid 5	3-D Coupled-Field Solid	8	UX, UY, UZ, VOLT for KEYOPT(1) = 3

The beam FE model without PVDF elements has passed the convergence test in terms of natural frequencies within ±1% errors for the first four modes. The same element mesh plan in beam that there are 45 divisions in beam length, 4 divisions in beam width, and 1 division in thickness is adopted. The mesh of PVDF film thus complies with the beam accordingly as shown in Fig. 3.

The displacement constraints of the finite element model are applied to those nodes at the fixed end for all DOFs as zero to fit the boundary conditions. For modal analysis, there is no need to specify loading conditions. The point force with 1 N is applied at the first location of PVDF sensor for harmonic response analysis in order to determine the FRFs between each PVDF sensor and the point force. The loading condition is simulated the same as the actual force applied in EMA discussed in next section.

4. EXPERIMENTAL MODAL ANALYSIS

The conventional modal testing procedure is adopted to perform the experimental modal analysis. Only the PVDF sensors are replaced instead of accelerometers. Figure 4 shows the substance picture for the cantilever beam adhered with evenly distributed PVDF sensors. The experimental equipment layout is also depicted and shown in Fig. 5. The hammer is actuated at position 1 and fixed to excite the structure. The PVDF sensors measure the beam response. The 4-channel FFT analyzer (SIG Lab) is used to capture the input force of the hammer actuator and the output voltage of PVDF sensors, respectively, and calculates FRF. Let the hammer actuator be fixed and the PVDF sensors be roving. A column of FRFs matrix can then be measured and transported to computer through the SCSI interface. The general-purpose curve fitting software, ME'scopeVES, is used to extract the system modal parameters. Natural frequencies, modal damping ratios

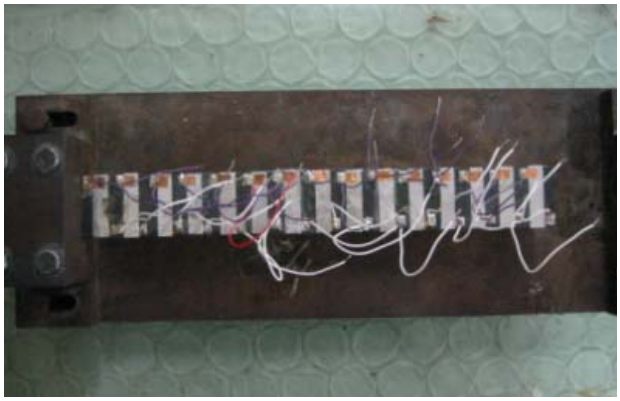

Fig. 4 The substance picture

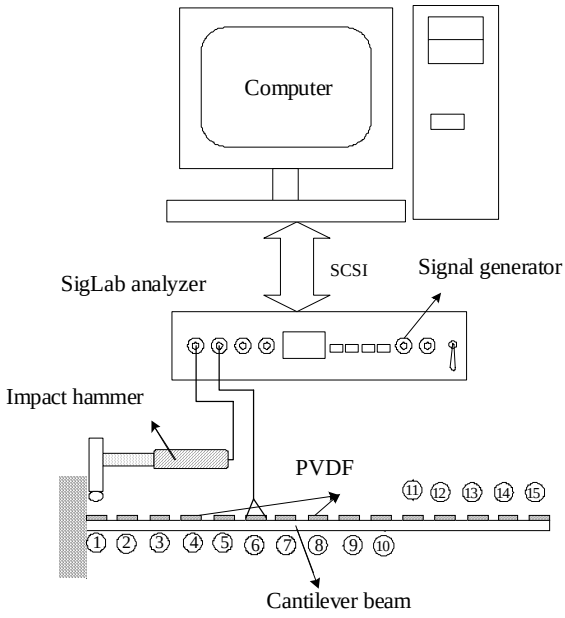

Fig. 5 Experimental equipment layout

and PVDF mode shape functions of the beam can be extracted. It is noted that the physical quantity of the PVDF sensor mode shape is voltage, and its physical meaning is proportional to the slope difference between the two edges of PVDF film as shown in Eq. (7).

5. RESULTS AND DISCUSSIONS

This section will present and compare the results from theoretical, finite element and experimental analyses.

5.1 Verification of Frequency Response Functions

Figure 6 shows the typical point FRF $\alpha_{v_i f_j}$ for i=1, j = 1, *i.e.* the sensing location is the same as the actuation one. There are four FRF spectral lines, including experimental, synthesized, FEA and theoretical ones, in the plots. Some observation and discussions are as follows:

1. For the point FRFs, there correctly appear anti-resonance points between resonance peaks for all of the four FRFs as expected.
2. The most discrepancy of FRFs as observed is between both the theoretical and experimental FRFs. The cause for the shift of anti-resonance points and the discrepancy of FRF shapes is that the theoretical model as described in Section 2 neglects the mass effect of PVDF sensor.
3. The FRF determined from FEA with the assumption of modal damping ratios 0.3% for all modes appears quite good agreement to the experimental one except only a slight shift near the fifth mode. It should also be noted that the PVDF mass is accounted for its effect during solution in FEA.
4. The synthesized FRF is regenerated with the extracted modal parameters, which will be shown in the next section, from curve-fitting process. That the synthesized FRF matches well with the experimental one indicates the success in the curve-fitting process.

In summary, the resonance frequencies and the shape of FRFs show reasonably good agreement between the experimental and finite element analysis. The bad agreement of theoretical FRF is mainly due to the neglect of PVDF mass effect. A refined modeling technique to include PVDF mass effect into the theoretical model can be desired and out of the content for this work.

5.2 Verification of Modal Parameters

Table 4 shows the comparison of natural frequencies obtained from theoretical, experimental and FEA results for the first four modes. The error percentages between experimental and FEA are within ±2%. On the other hand, the theoretical natural frequencies reveal slightly higher error percentage −2.86% at the first modes. This can be the mass effect of PVDF sensors. The FEA works well in predicting the natural frequencies of the beam with distributed PVDF sensors.

The modal damping ratios extracted through the curve-fitting process are shown in Table 5. The modal damping ratios are about 0.324% ~ 0.518%, slightly

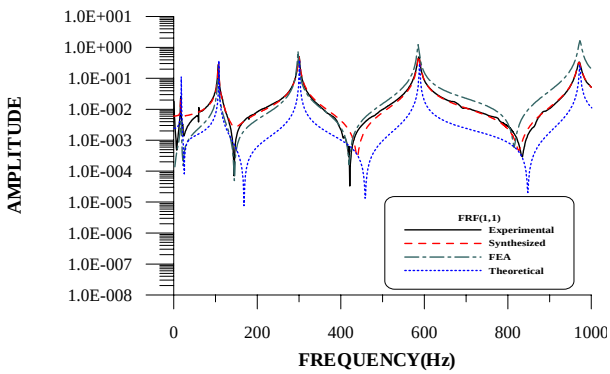

Fig. 6 Frequency response functions for i = 1, j = 1

higher than 0.1% ~ 0.5% for steel material. The adhesion and material effect of PVDF films can contribute to increase the damping ratio. It is also noted that structural damping can not be determined from theoretical or finite element analysis.

Figures 7(a) and 7(d) show the first four bending mode shapes of the beam adhered with PVDF sensors from FEA. It is interested to note that the displacement mode shapes reveal as expected for cantilever beam characteristics. However, the voltage output of a PVDF sensor is proportional to the slope difference between the two edges of the PVDF film as shown in Eq. (7). It is also noted that fixed hammer actuator and roving PVDF sensors are adopted to perform the FRF measurement. Therefore, the PVDF mode shapes can be extracted through the curve-fitting process. The first four theoretical, experimental and FEA PVDF sensor mode shapes of the cantilever beam are depicted in Figs. 8(a)~8(d). In Fig. 8, the physical quantities of "amplitude" are voltages for FEA, EMA or theoretical solutions. As shown in Eq. (7), $\phi_{n,i}^{v}$ represents the values of the *n*-th PVDF sensor mode shape functions at the *i*-th location of the PVDF sensor. The physical quantity of the PVDF sensor mode shape is voltage, and the physical meaning of the PVDF sensor mode shape is proportional to the slope difference between the two edges of PVDF film as shown in Eq. (7). For FEA, the voltage output of a PVDF sensor can be extracted from the PVDF element (SOLID5), although the structural displacement mode shapes can be as shown in Fig. 7. One can observe that those mode shapes agree reasonably well. The PVDF slope sensor mode shapes appear as the mirror image of displacement mode shape against the clamped end [18]. The applications of FEA and EMA to vibration analysis of the beam structure integrated with PVDF sensors is demonstrated and shown promising.

MAC (modal assurance criterion) [23] for the comparison among the theoretical, experimental and FEA mode shapes are tabulated in Tables 6(a) ~ 6(c). Table 6(a) shows the MAC matrix between FEA and theoretical mode shapes. That the diagonal elements of MAC matrix reveal the values larger than 0.97 and close to one indicates very good agreement between the FEA and theoretical PVDF sensor mode shapes. The off-diagonal elements of MAC matrix near to zero indicate the orthogonality of mode shapes. Similarly, Tables 6(b) and 6(c) show the MAC matrices for between FEA and experimental mode shapes and between theoretical and experimental mode shapes, respectively. One can also observe that diagonal elements of MAC matrix are generally larger than 0.9, except the first mode, and the off-diagonal elements are near zero.

Table 4 Comparison the natural frequencies of cantilever beam

Natural frequency (Hz)	f_1	f_2	f_3	f_4
Experimental	16.6	107	300	587
FEA	16.92	106.01	297.52	585.54
Error percentage	1.94%	–0.93%	–0.83%	–0.25%
Theoretical	17.089	107.097	299.877	587.642
Error percentage	–2.861%	0.091%	–0.041%	0.109%

Table 5 The experimental modal damping of cantilever beam

Mode	Modify damping ratio (%)
ξ_1	0.390
ξ_2	0.518
ξ_3	0.499
ξ_4	0.324

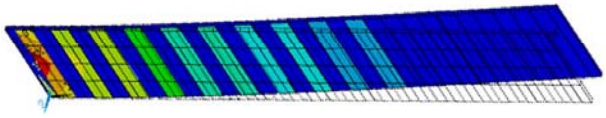

(a) first bending mode

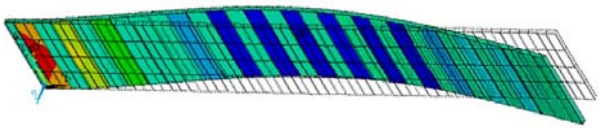

(b) second bending mode

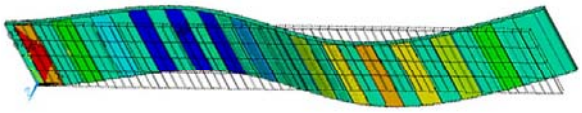

(c) third bending mode

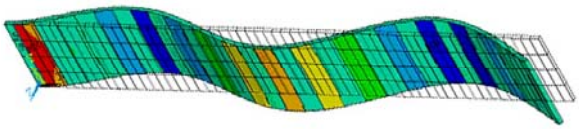

(d) fourth bending mode

Fig. 7 The PVDF sensors mode shape of the cantilever beam from EMA

6. CONCLUSIONS

This paper presents the FEA for cantilever beam adhered with distributed PVDF sensors. Both FRFs and

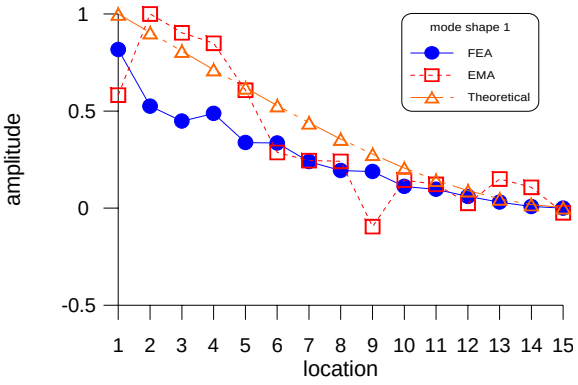

(a) mode 1

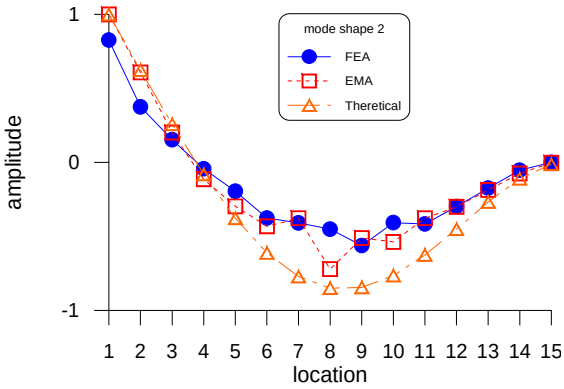

(b) mode 2

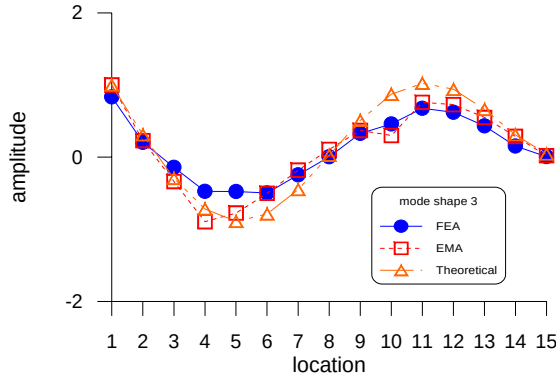

(c) mode 3

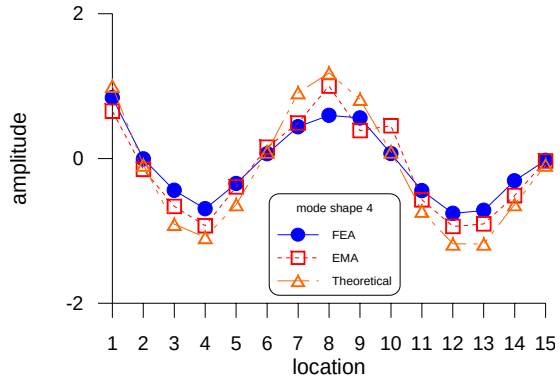

(d) mode 4

Fig. 8 The PVDF sensors mode shape of the cantilever beam

Table 6 MAC matrix of mode shape

(a) MAC matrix between FEA and theoretical mode shapes

Mode	1	2	3	4
1	**0.97289**	0.00405	0.00338	0.00031
2	0.00736	**0.97177**	0.00049	0.00372
3	0.00557	0.00179	**0.97815**	0.00002
4	0.00252	0.00600	0.00083	**0.97038**

(b) MAC matrix between FEA and experimental mode shapes

Mode	1	2	3	4
1	**0.74727**	0.02117	0.01756	0.05388
2	0.04233	**0.94018**	0.02506	0.02582
3	0.00445	0.01009	**0.9277**	0.02669
4	0.00229	0.00466	0.00597	**0.8775**

(c) MAC matrix between theoretical and experimental mode shapes

Mode	1	2	3	4
1	**0.88982**	0.00229	0.01054	0.06464
2	0.01784	**0.92607**	0.00934	0.00281
3	0.00241	0.00372	**0.90850**	0.01226
4	0.00488	0.00498	0.00647	**0.91477**

modal parameters are determined and validated via theoretical analysis and experimental modal testing. The conventional EMA procedure is adopted with the use of PVDF sensors and impact hammer actuator. The fixed actuator and roving PVDF sensor is adopted to EMA for measuring FRFs, and so forth structural modal parameters can be extracted through curve-fitting process. Results show that three kinds of analysis, *i.e.* FEA, EMA and theoretical analysis, agree reasonably well. In particular, the extracted mode shapes can be interpreted as the PVDF sensor mode shape, *i.e.* proportional to the slope difference between two edges of the PVDF sensor. The developed analysis methodology can be extended to other complex structures. The idea of smart structural test (SST) is theoretically and experimentally demonstrated.

ACKNOWLEDGMENT

This work was supported by National Science Council, Taiwan, under contract number NSC 91-2212-E-020-003.

NOMENCLATURE

A_v	the area of PVDF sensor
b_b	beam width
c^E	elastic constant by fixed the electric field
D	electric displacement of piezoelectric material
E	electrical field of piezoelectric material
e	piezoelectric stress constant
e_{31}, e_{32}	piezoelectric field intensity constants
E_b	Young's Modulus of beam
F_j	the j-th impact force amplitude
f_n	the n-th natural frequency of beam
I_b	cross sectional moment of inertia of the beam
L_b	beam length
l_v	the width PVDF sensor

S	mechanical strain of piezoelectric material
T	mechanical stress of piezoelectric material
t_b	beam thickness
t_v	thickness of the PVDF film
V_i	the *i*-th PVDF voltage
x_{f_j}	the location of the *j*-th hammer actuator in *x*- and *y*- coordinates
x_{v1_i}, x_{v2_i}	the location of the *i*-th PVDF sensor in *x*-coordinate
α_n	the characteristic values
$\alpha_{v_i f_j}$	the FRF between the voltage of the *i*-th PVDF sensor and the force amplitude of the *j*-th hammer actuator
ω	excitation frequency
ω_n	the *n*-th natural frequency of beam
ρ_b	beam density
ε	the permittivity of the PVDF sensor
ε^S	permittivity constant by fixed the strain
ξ_n	the *n*-th modal damping ratio of beam
ϕ_n	the *n*-th displacement mode shape of beam
$\phi^v_{n,i}$	the *n*-th PVDF mode shape function of beam at the *i*-th location of the PVDF sensor
$\phi^f_{n,j}$	the *n*-th hammer mode shape function of beam at the *j*-th location of the hammer actuator

REFERENCE

1. Hubbard, J. E., "Distributed Sensors and Actuators for Vibration Control in Elastic Components," *Noise-Con 87*, State College, PA, pp. 407–412 (1987).
2. Lee, C. K. and Moon, F. C., "Modal Sensors/Actuators," *Journal of Applied Mechanics*, 57, pp. 434–441 (1990).
3. Collins, S. A., Padilla, C. E., Notestine, R. J., von Flotow, A. H., Schmitz, E. and Ramey, M., "Design, Manufacture, and Application to Space Robotics of Distributed Piezoelectric Film Sensors," *Journal of Guidance Control*, 15, pp. 396–403 (1992).
4. Galea, S. C., Chiu, W. K. and Paul, J. J., "Use of Piezoelectric Films in Detecting and Monitoring Damage in Composites," *Journal of Intelligent Material Systems and Structures*, 4, pp. 330–336 (1993).
5. Collet, M. and Jezequel, L., "A New Approach to Modal Filtering with Laminated Piezo-electric Sensors," *Proceedings for the 12th International Modal Analysis Conference*, Nashville, TN, pp. 246–254 (1994).
6. Tanaka, N., Snyder, S. D. and Hansen, C. H., "Distributed Parameter Modal Filtering Using Smart Sensors," *Transactions of the ASME Journal of Vibration and Acoustics*, 118, pp. 630–640 (1996).
7. Allik, H. and Hughes, T. J. R., "Finite Element Method for Piezoelectric Vibration," *International Journal for Numerical Methods in Engineering*, 2, pp. 151–157 (1970).
8. Boucher, D., Lagier, M. and Maerfeld, C., "Computation of the Vibrational Modes for Piezoelectric Array Transducers Using a Mixed Finite Element-Perturbation Method," *IEEE Transactions on Sonics and Ultrasonics*, Su-28(5), pp. 318–330 (1981).
9. Kunkel, H. A., Locke, S. and Pikeroen, B., "Finite-Element Analysis of Vibrational Modes in Piezoelectric Ceramic Disks," *IEEE Transactions on Ultrasonics, Ferroelectrics, and Frequency Control*, 37(4), pp. 316–328 (1990).
10. Ha, S. K., Keilers, C. and Chang, F. K., "Finite Element Analysis of Composite Structures Containing Distributed Piezoceramic Sensors and Actuators," *AIAA Journal*, 30(3), pp. 772–780 (1992).
11. Kagawa, Y. and Yamabuchi, T., "Finite Element Simulation of a Composite Piezoelectric Ultrasonic Transducer," *IEEE Transactions on Sonics and Ultrasonics*, Su-26(2), pp. 81–88 (1979).
12. Challande, C., "Optimizing Ultrasonic Transducers Based on Piezoelectric Composites Using a Finite-Element Method," *IEEE Transducers on Ultrasonics, Ferroelectrics, and Frequency Control*, 37(2), pp. 135–140 (1990).
13. Tsuchiya, T. and Kagawa, Y., "Finite Element Simulation of Piezoelectric Transducers," *IEEE Transducers on Ultrasonics, Ferroelectrics, and Frequency Control*, 48(4), pp. 872–878 (2001).
14. Sun, F. P., Liang, C. and Rogers, C. A., "Experimental Modal Testing Using Piezoceramic Patches as Collocated Sensor-Actuators," *Proceedings of the 1994 SEM Spring Conference and Exhibits*, Baltimore, Maryland, pp. 871–879 (1994).
15. Norwood, C., "The Measurement of Natural Frequencies and Mode Shapes of Submerged Cylinders Using PVDF Strip Excitation," *Proceedings of Inter-Noise 95*, Newport Beach, CA, pp. 1337–1340 (1995).
16. Wang, B. T., "Characterization of Transfer Functions for Piezoceramic and Conventional Transducers," *Journal of Intelligent Material Systems and Structures*, 7, pp. 390–398 (1996).
17. Wang, B. T., "Structural Modal Testing with Various Actuators and Sensors," *Mechanical System and Signal Processing*, 12(5), pp. 627–639 (1998).
18. Wang, B. T. and Wang, C. C., "Feasibility Analysis of Using Piezoceramic Transducers for Cantilever Beam Modal Testing," *Smart Materials and Structures*, 6, pp. 1–11 (1997).
19. Wang, B. T., "The PVDF Based Wavenumber Domain Sensing Techniques for Active Sound Radiation of a Simply-Supported Beam," *Journal of Acoustical Society of America*, 103(4), pp. 1904–1915 (1998).
20. Meirovich, L., *Elements of Vibration Analysis*, McGraw-Hill Book Company, New York (1986).
21. Blevins, R. D., *Formulas for Natural Frequency and Mode Shape*, Van Nostrand, New York (1979).
22. ANSI/IEEE Std 176–1987, *IEEE Standard on Piezoelectric*, American National Standards Institute (1987).
23. Ewins, D. J., *Modal Testing: Theory and Practice*, Research Studies Press LTD., Letchworth Hertfordshire, England (1986).

(Manuscript received February 20, 2004, accepted for publication September 9, 2005.)